Contributions to Mineralogy and Petrology (2018) 173:106
https://doi.org/10.1007/s00410-018-1534-6

ORIGINAL PAPER

Composition of barian mica in multiphase solid inclusions from orogenic garnet peridotites as evidence of mantle metasomatism in a subduction zone setting

Renata Čopjaková[1] · **Jana Kotková**[2]

Received: 13 June 2018 / Accepted: 9 November 2018 / Published online: 27 November 2018

Abstract

Multiphase solid inclusions in minerals formed at ultra-high-pressure (UHP) provide evidence for the presence of fluids during deep subduction. This study focuses on barian mica, which is a common phase in multiphase solid inclusions enclosed in garnet from mantle-derived UHP garnet peridotites in the Saxothuringian basement of the northern Bohemian Massif. The documented compositional variability and substitution trends provide constraints on crystallization medium of the barian mica and allow making inferences on its source. Barian mica in the multiphase solid inclusions belongs to trioctahedral micas and represents a solid solution of phlogopite $KMg_3(Si_3Al)O_{10}(OH)_2$, kinoshitalite $BaMg_3(Al_2Si_2)O_{10}(OH)_2$ and ferrokinoshitalite $BaFe_3(Al_2Si_2)O_{10}(OH)_2$. In addition to Ba (0.24–0.67 apfu), mica is significantly enriched in Mg (X_{Mg} ~ 0.85 to 0.95), Cr (0.03–0.43 apfu) and Cl (0.04–0.34 apfu). The substitution vector involving Ba in the I-site which describes the observed chemical variability can be expressed as $BaFe^{IV}AlClK_{-1}Mg_{-1}Si_{-1}(OH)_{-1}$. A minor amount of Cr and ^{VI}Al enters octahedral sites following a substitution vector $^{VI}(Cr,Al)_2\square^{VI}(Mg,Fe)_{-3}$ towards chromphyllite and muscovite. As demonstrated by variable Ba and Cl contents positively correlating with Fe, barian mica composition is partly controlled by its crystal structure. Textural evidence shows that barian mica, together with other minerals in multiphase solid inclusions, crystallized from fluids trapped during garnet growth. The unusual chemical composition of mica reflects the mixing of two distinct sources: (1) an internal source, i.e. the host peridotite and its garnet, providing Mg, Fe, Al, Cr, and (2) an external source, represented by crustal-derived subduction-zone fluids supplying Ba, K and Cl. At UHP–UHT conditions recorded by the associated diamond-bearing metasediments (c. 1100 °C and 4.5 GPa) located above the second critical point in the pelitic system, the produced subduction-zone fluids transporting the elements into the overlying mantle wedge had a solute-rich composition with properties of a hydrous melt. The occurrence of barian mica with a specific chemistry in barium-poor mantle rocks demonstrates the importance of its thorough chemical characterization.

Keywords Ba-rich phlogopite · Kinoshitalite · Multiphase solid inclusions · Orogenic garnet peridotite · Metasomatism · Bohemian Massif

Introduction

Subduction zones represent sites where chemical components are recycled from the subducting slab into the supra-subduction mantle wedge, triggering mantle metasomatism and its partial melting (e.g. Spandler and Pirard 2013). The transfer of slab-derived elements, namely LILE and LREE, but also of U and Th, is mediated by fluids/melts/supercritical fluids (hereinafter "fluids") (Hermann et al. 2006; Manning 2004; Keppler 2017). Ultrahigh-pressure metamorphic (UHPM) terranes which involve slices of deeply subducted crustal rocks as well as orogenic garnet peridotites (e.g. Liou

Communicated by Daniela Rubatto.

✉ Renata Čopjaková
copjakova@sci.muni.cz

[1] Department of Geological Sciences, Masaryk University, Kotlářská 2, 611 37 Brno, Czech Republic

[2] Czech Geological Survey, Klárov 3, 118 21 Prague 1, Czech Republic

et al. 2009) represent a window for studying crust-mantle interaction including element transfer.

We focused on a UHPM terrane in the Saxothuringian domain of the northern Bohemian Massif in the European Variscan belt, where garnet peridotites are associated with diamond- and coesite-bearing crustal-derived metamorphic rocks. As these rocks show mineral assemblages similar to high-pressure granulites, the presence of UHP mineral indicators (diamond, coesite) provides an explanation for the common peridotite–granulite association within the European Variscides by deep crustal subduction of the crustal rocks into mantle depths (Kotková et al. 2011). Multiple solid inclusions (MSI) discovered in garnet provide evidence for crustal metasomatism of the studied garnet peridotites, whereas only cryptic but not modal metasomatism is documented in the host rock (Medaris et al. 2015). These inclusions are dominated by Ba-rich mica, carbonate and amphibole.

Divalent Ba^{2+} substitutes for univalent K^{+} in the interlayer cation sites of micas, with higher Ba concentrations in trioctahedral micas compared to dioctahedral micas. Trioctahedral micas include kinoshitalite $BaMg_3(Al_2Si_2)O_{10}(OH)_2$, ferrokinoshitalite $BaFe_3(Al_2Si_2)O_{10}(OH)_2$, oxykinoshitalite $Ba(Mg_2Ti^{4+})(Al_2Si_2)O_{10}O_2$ and anandite $BaFe^{2+}{}_3(Fe^{3+}Si_3)O_{10}S(OH)$ (Pattiaratch et al. 1967; Yoshii et al. 1973; Frimmel et al. 1995; Kogarko et al. 2005). Trioctahedral barian micas have been described in several types of SiO_2-deficient rock types with two main modes of formation. Magmatic barian micas occurring in potassic and alkaline magmatic rocks (nephelinites, leucitites, carbonatites) and kimberlites form in the final stages of magma evolution from residual melt enriched in volatiles (e.g. Mansker et al. 1979; Gaspar and Wyllie 1982; Edgar 1992; Zhang et al. 1993; Shaw and Penczak 1996; Solovova et al. 2009; Zurevinski and Mitchell 2011). Barian biotite to kinoshitalite/ferrokinoshitalite described from Mn or Fe deposits, calc-silicate rocks, and marbles is attributed to metasomatism by Ba-bearing fluids likely derived from barite-bearing sediments at amphibolite- to granulite-facies metamorphic conditions (e.g. Bol et al. 1989; Dasgupta et al. 1989; Solie and Su 1987; Gnos and Armbruster 2000; Tracy and Beard 2003). Reports on Ba-rich mica formed due to subduction-related metasomatism, such as ferrokinoshitalite in peridotite (Tumiati at al. 2007) or Ba-rich biotite in calcic gneiss (Majka et al. 2015), are much more rare.

This paper presents the results from a study of Ba-rich phlogopite to kinoshitalite, occurring in multiphase solid inclusions enclosed in garnet in UHP garnet peridotites in the Saxothuringian basement of northern Bohemia. We describe the compositional variability and substitution trends in barian mica aiming to characterize their crystallization medium, and demonstrate that this approach is capable of unravelling signatures of mantle metasomatism by fluids derived from the subducting crustal slab. We show that Ba can occur in mica despite the Ba-poor character of the host rocks.

Geological background

The investigated garnet peridotites come from the T-7 borehole, located near the village of Staré (50°28.85′N, 13°53.65′E; Fig. 1) in northern Bohemia. It was drilled into the Saxothuringian basement, which is largely covered by Cretaceous platform deposits and Cenozoic volcanic and sedimentary rocks (Fig. 1). The Saxothuringian basement involving UHP–UHT diamond-bearing garnet–phengite gneiss, coesite-bearing eclogite and garnet peridotite is exposed in the Erzgebirge further to the northwest

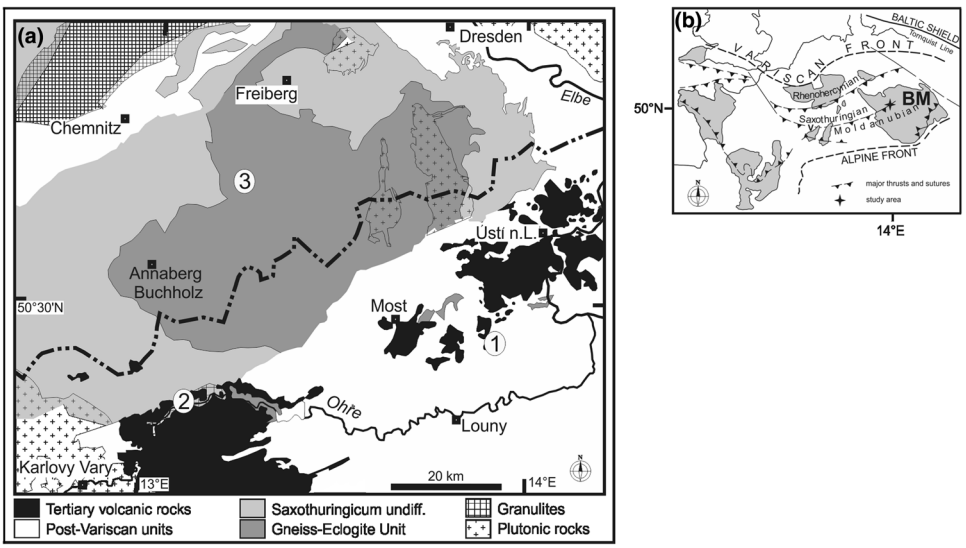

Fig. 1 **a** Geological sketch map of the northern Bohemian Massif with the location of the T-7 borehole (1). Outcrops of the Eger Crystalline Complex (2) and diamond-bearing UHPM rocks of the Erzgebirge (3) are also shown. undiff.—undifferentiated, i.e., phyllite and micaschist eclogite units; n.L.—nad Labem (on the Elbe River). **b** Study area location within the European Variscan belt. BM—Bohemian Massif (adapted after Kotková et al. 2011)

(Schmädicke et al. 1992; Schmädicke and Evans 1997; Massonne 2003).

The T-7 borehole intersects an inclined garnet peridotite body (c. 114 metres thick, a 228-m drillcore section) consisting of alternating layers of harzburgite and lherzolite with subordinate garnet pyroxenite and eclogite, hosted by high-pressure granulite (see Kopecký and Sattran 1966; Kopecký and Paděra 1974; Kotková 1993 for the borehole description and geological section). This granulite forms a hidden ENE–WSW lense-shaped body hosted by paragneisses, whereas another elongated granulite body within orthogneisses is partly exposed in the erosion window of the Eger River valley towards WSW (Mlčoch and Konopásek 2010). Diamond and coesite discovered in both of these high-pressure granulite bodies document the UHP conditions experienced by these crustal rocks (Kotková et al. 2011).

Geothermobarometry and thermodynamic modelling yielded similar UHP–UHT conditions for both the mantle and crustal rocks, estimated at 1030–1150 °C/3.6–4.8 GPa for garnet peridotite, 900–1050 °C/3.5–4.5 GPa for the associated kyanite eclogite, and ≥ 1100 °C and 4.5 GPa for UHP diamond-bearing rock (Kotková and Janák 2015; Medaris et al. 2015; Haifler and Kotková 2016). The rock complex was rapidly exhumed along an initial near-isothermal decompressional path at a rate of about 1.5 cm/yr with subsequent rapid cooling reflected by overlapping U–Pb zircon and rutile and Ar–Ar biotite ages from the HP granulites and associated orthogneisses in the outcrop area (Kotková et al. 1996, 2016; Zulauf et al. 2002; Haifler and Kotková 2016).

The garnet peridotite represents a fertile to slightly depleted lithospheric mantle, with lithological banding attributed to the active continental margin deformation. Trace element and isotopic data suggest cryptic metasomatism by subduction-related fluids (Medaris et al. 2015). Based on the P–T evolution, including preserved relics of prograde mineral assemblage in the T-7 eclogite, and geochemical characteristics, it has been proposed that the garnet peridotites were derived from a subcontinental mantle wedge and plausibly involved in the subduction as well (Schmädicke and Evans 1997; Group III of; Medaris et al. 2005; Kotková and Janák 2015). The rock assemblage of the T-7 borehole thus represents a unique opportunity for studying material transfer in a deep subduction zone environment.

Analytical methods

Scanning electron microscope FEG–SEM Tescan Mira3GMU (Czech Geological Survey, Prague) equipped with EDS X-MaxN 80 detector (Oxford Instruments) was used for imaging of the multiple solid inclusions at accelerating voltage 15 kV and probe current of 1.8 nA. Modal amounts of barian mica (in %) present within the MSI was calculated from the phase maps. These were acquired using the parameters of boundary tolerance 3.0 and grouping level 2.0 from X-ray elemental maps of the MSI using Aztec 3.3 software (at 1000s live time, 20 kV energy range with 10 V/channel energy resolution).

The chemical analyses of minerals were performed using a Cameca SX100 electron microprobe (EMP) in wavelength dispersive mode at the Joint Laboratory of Electron Microscopy and Microanalysis of the Department of Geological Sciences of Masaryk University and Czech Geological Survey in Brno. The operating conditions for the analyses were as follows: an accelerating voltage of 15 kV, a beam current of 10 nA and a beam diameter of 1–5 µm. The natural and synthetic standards used involve: Si, Al, K—sanidine; Ca—wollastonite, Na—albite; Mg—pyrope; Fe—almandine; Mn—spessartine; Ti—titanite; Zn—$ZnAl_2O_4$; Ni—Ni_2SiO_4; V—$ScVO_4$; Ba—$BaSO_4$; Sr—$SrSO_4$; F—topas; Cl—vanadinite. The raw data were reduced using the X-Phi matrix correction procedure (Merlet 1994).

The barium concentration in whole rocks was determined by ICP–MS at the Czech Geological Survey in Prague in the Czech Republic.

Sample description, bulk rock composition and mineral chemistry

We investigated barian mica-bearing multiphase solid inclusions in garnet from five samples of garnet peridotites—three lherzolites (from a depth of 282 m, 313 m and 332 m in the T-7 borehole section) and two harzburgites (276 m and 322 m). The bulk rock geochemistry of these rocks as well as their modal analyses and mineral compositions of major rock-forming minerals were presented by Medaris et al. (2015). Based on the contents of major and trace elements, lherzolites 282 and 313 are similar in composition to the primitive mantle. Llherzolite 332 and harzburgites are slightly depleted, with low contents of TiO_2, Al_2O_3, and CaO, and LREE enrichment accompanied by HREE depletion. These are interpreted as residues from the partial melting of primitive lherzolite followed by cryptic metasomatism (Medaris et al. 2015). The barium contents in peridotites are very low (˂ 0.3–100 ppm, this paper, Table 1).

In the lherzolite as well as harzburgite, the garnet porphyroclasts reaching up to 5 mm in size are irregularly distributed in a fine-grained (≤ 1 mm) extensively serpentinized granoblastic matrix consisting of olivine, orthopyroxene and clinopyroxene (Fig. 2). Garnet in lherzolites is relatively preserved, only being locally rimmed by amphibole + phlogopite + magnetite + calcite in some cases (Fig. 2d), whereas garnet in harzburgite is to a variable degree consumed by kelyphite composed of spinel clinopyroxene and orthopyroxene (Fig. 2c). Garnets are transected by thin calcite veins and cracks filled with late serpentine.

Table 1 Barium contents in whole rock samples (detection limit 0.3 ppm) and observed mineral assemblage in MSI

Sample	Rock	Ba in whole rock (ppm)	Mineral asseblage in MSI			Kns in MSI	
			Major minerals	Minor minerals	Accessory minerals	Min–max/μ [%]	*n*
313	lherzolite	< 0.3	Hbl, Mgs, Kns, Dol	Spl, Cpx	Ap, Thr/Urn, Pn, Sch, Ccp	0.0–41.1/10.1	24
282	lherzolite	40	Hbl, Kns, Mgs, Dol	Spl, Gr	Ap, Pn, Thr/Urn	7.2–30.2/17.4	4
332	lherzolite	90	Kns, Hbl, Dol, Mgs	Cpx, Nrs, Grt II	Thr/Urn, Mnz, Ap, Pn, Gn	9.5–73.7/28.7	9
322	harzburgite	100	Kns, Dol, Cpx	Mgs, Opx, Grt II	Nrs, Chr, Mnz, Sch	10.9–64.6/31.0	11
276	harzburgite	n.a.	Hbl, Kns, Dol	Grt II, Mgs, Opx	Mnz, Thr/Urn, Pn	12.6–45.3/26.5	10

Mineral proportions decrease from major via minor to accessory, and their modal amount further decreases from the left to the right in these groups. Minimum (min), maximum (max) and average (μ) modal amount of barian mica (Kns) in MSI determined from several (n) MSI in each rock sample are also reported

Used abbreviations for minerals: *Kns* barian phlogopite to kinoshitalite, *Hbl* amphibole, *Cpx* clinopyroxene, *Opx* orthopyroxene, *Grt* garnet, *Mgs* magnesite, *Dol* dolomite, *Nrs* norsethite, *Spl* spinel, *Chr* chromite, *Thr* thorianite, *Urn* uraninite, *Gr* graphite, *Mnz* monazite, *Ap* apatite, *Sch* scheelite, *Pn* pentlandite, *Gn* galena, *Ccp* chalcopyrite

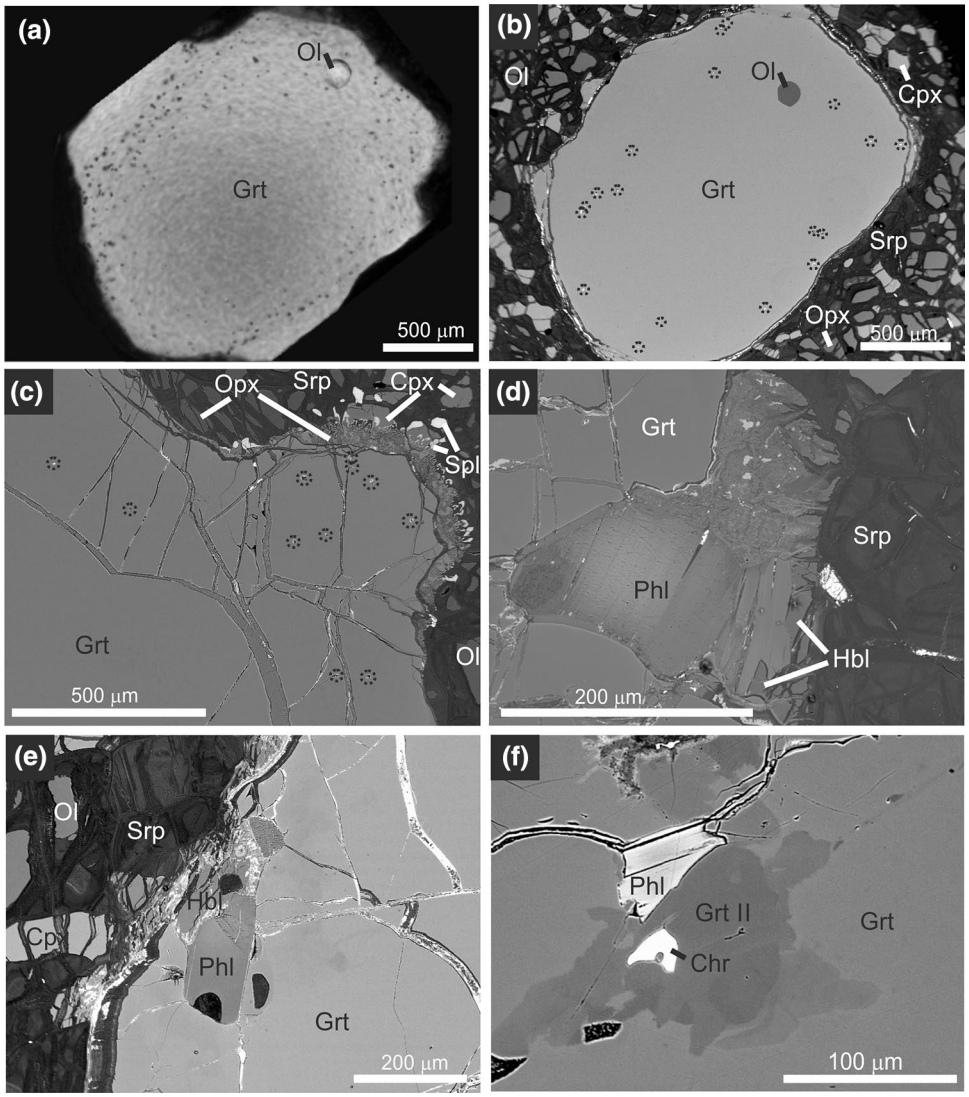

Fig. 2 BSE images showing textural relations of minerals and MSI; **a** Distribution of MSI in an annulus at the garnet rim, lherzolite 332. The image was produced by stacking five images taken at different depths of a 200-μm-thick polished section using the Helicon Focus software. **b** BSE image of the same garnet with marked MSI exposed on the polished surface. The MSI are marked by black dotted circles. **c** BSE image of garnet from harzburgite 322, consumed locally by kelyphite, with MSI exposed on the polished surface marked by black dotted circles. **d** BSE image of phlogopite + amphibole replacing garnet in lherzolite 332. **e** BSE image of phlogopite associated with amphibole close to the garnet rim in lherzolite 313. **f** Phlogopite associated with chromite and garnet II in harzburgite 322. For abbreviations of rock-forming minerals see Table 1. *Phl* phlogopite

Olivine composition corresponds to forsterite (X_{Mg} = 0.90–0.92), orthopyroxene is enstatite (X_{Mg} = 0.91–0.92), and clinopyroxene is diopside (X_{Mg} = 0.92–0.94, Cr ~ 1.0 wt% Cr_2O_3). Garnet is Mg-rich, with 2.04–2.23 and 1.96–2.11 apfu Mg and X_{Mg} = 0.79–0.84 and 0.81–0.85 in lherzolite and harzburgite, respectively, and contains a relatively high amount of Cr (0.09–0.15 resp. 0.34–0.48 apfu Cr). It typically shows a large chemically homogeneous core and about 250–500 µm wide rim with retrograde zoning features, i.e. Mg as well as X_{Mg} decrease and Fe, Al and Ca increase (Fig. 3a). Garnet in harzburgite is enriched in Cr, Ca and Fe and impoverished in Al and Mg at the rim (Fig. 3b), which reflects its consumption by the kelyphite. Serpentine-group minerals formed at the expense of the matrix phases (56–66 vol% of matrix minerals are serpentinized) and feature a variable X_{Mg} ratio (0.85–0.96) and minor amounts of Al (0.05–3.60 wt% Al_2O_3), Cr (≤ 2.09 wt% Cr_2O_3) and Ca (0.03–0.46 wt% CaO).

Multiphase solid inclusions

We documented multiphase solid inclusions in 90 garnet grains within 8 thin sections of both the lherzolite and harzburgite. The MSI are concentrated in a ~ 200 to 500 µm wide annulus at the rim of garnet (Fig. 2a), whereas the garnet cores are mostly inclusion-free, apart from rare rutile needles, and located away from fractures containing late serpentine. There are 10–25 MSI exposed on the polished garnet surface (Fig. 2b, c). Most of the MSI studied have a polygonal negative shape (Fig. 4). Their boundaries towards the host garnet can be straight or with embayments or acute tips. The MSI show equilibrium granular texture as well as intimate intergrowths of phases.

The multiphase solid inclusions in lherzolite are larger, and much more variable, compared to those in harzburgite. They reach 10–40 µm in size and typically contain amphibole (pargasite), barian mica, magnesite and dolomite in variable proportions (Table 1; Fig. 4a–d). Moreover, minor to accessory clinopyroxene (omphacite), garnet II, graphite, spinel, Cl-apatite, thorianite/uraninite, monazite, pentlandite, scheelite, galena, chalcopyrite and Ba-rich carbonate (norsethite) reaching only several microns in size occur in the MSI. The mineral assemblage of the relatively smaller MSI in harzburgite (10–20 µm) is usually simpler, represented mainly by dolomite and barian mica in variable amounts (Table 1; Fig. 4e, f). Moreover, clinopyroxene (omphacite), amphibole (pargasite), and minor orthopyroxene (enstatite), magnesite and garnet II may also be present. Tiny Ba-rich carbonate (norsethite), magnesiochromite, monazite, thorianite/uraninite, pentlandite and scheelite were also recognized.

Distribution of barian mica in peridotites and MSI

Barian mica represents a typical phase in the MSI, although its modal amount varies from sample to sample and even within a single garnet grain. It makes only in average ~ 10% of the MSI in lherzolite 313 but often more than 50% of the MSI in lherzolite 332 and harzburgite 322, and its modal amount correlates with the bulk rock Ba content (Table 1). In the MSI from lherzolite, barian mica commonly forms anhedral grains (Fig. 4a–d), which are intimately intergrown

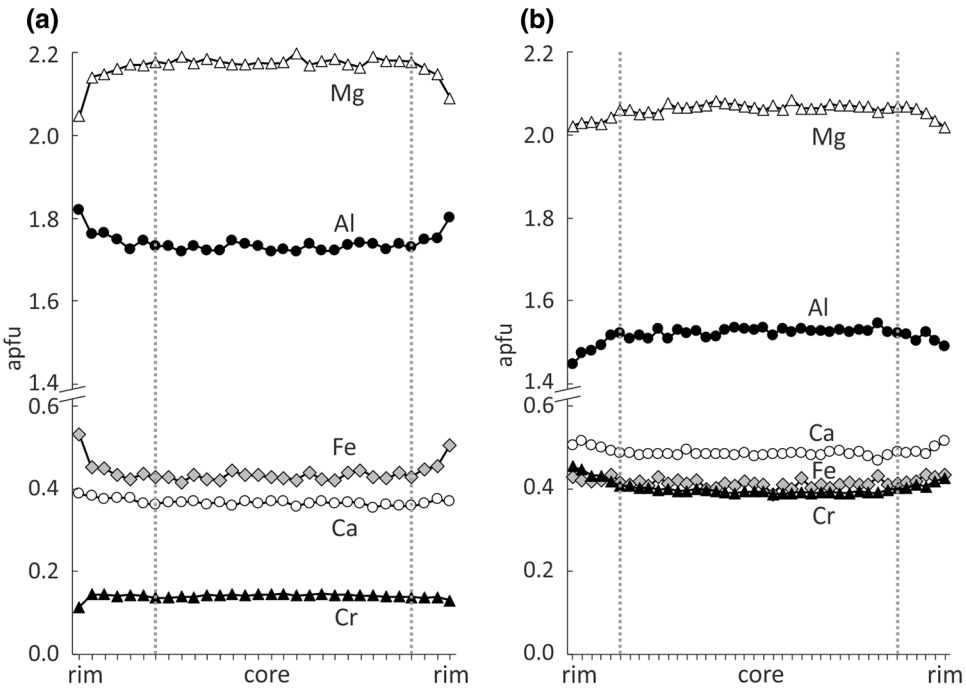

Fig. 3 Representative compositional profiles of garnets from **a** lherzolite 332 and **b** harzburgite 322. The step between analytical points was 60 and 40 µm, respectively. The dotted line marks the boundary between the MSI-rich annulus and the MSI-free inner part of garnet

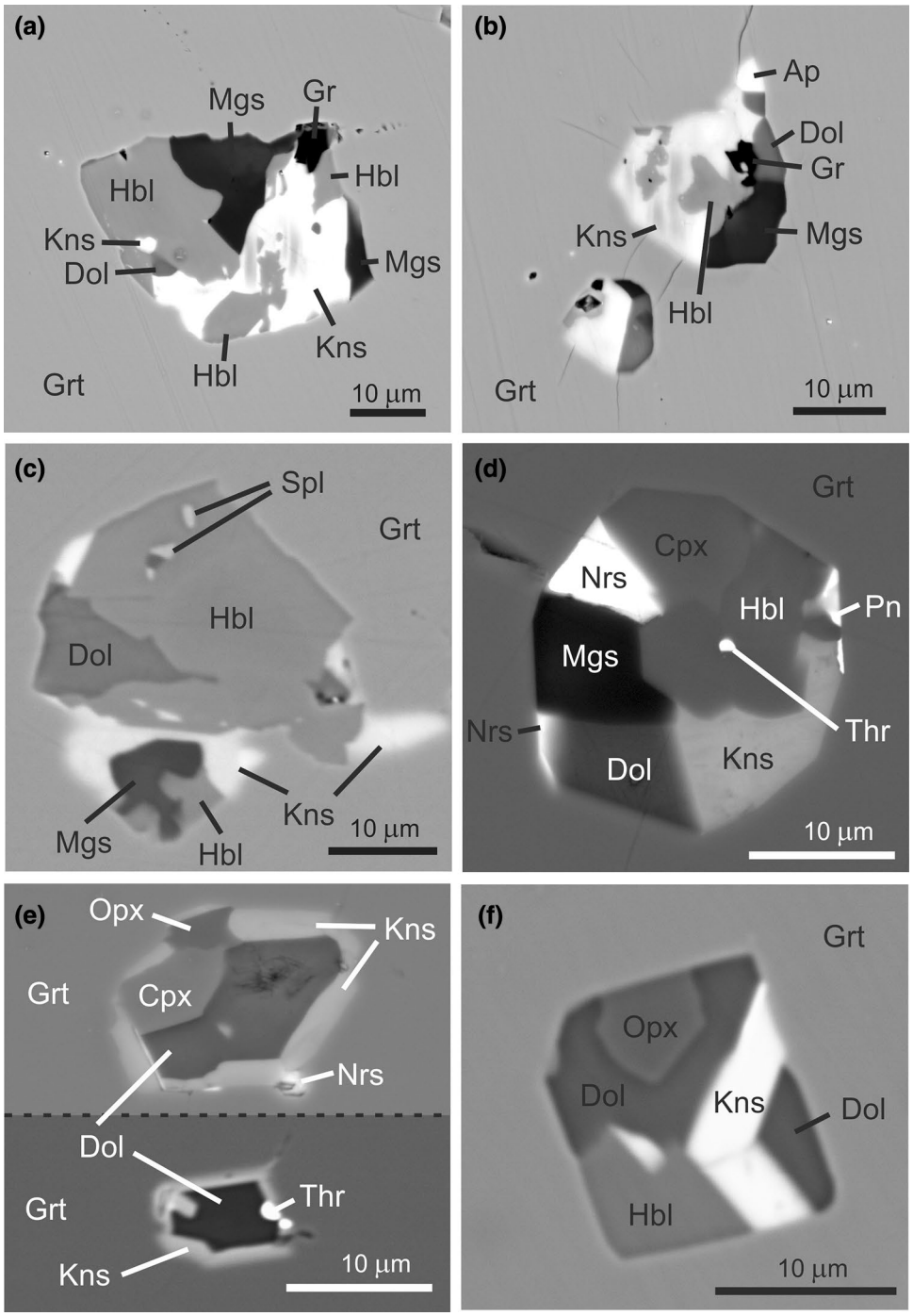

Fig. 4 BSE images of barian mica-bearing MSI in garnet from peridotites; **a, b** lherzolite 282; **c** lherzolite 313; **d** lherzolite 332; **e** harzburgite 322; **f** harzburgite 276. For abbreviations of minerals see Table 1

with other associated minerals, and it can show irregular zoning in BSE images (Fig. 4a, b). In harzburgite, barian mica commonly occurs at the rim of the MSI around a central dolomite (Fig. 4e) or it forms subhedral grains growing from the MSI rim inwards (Fig. 4e), and it appears chemically homogeneous in BSE images.

Trace amounts of phlogopite occur at the garnet rims. In lherzolite, phlogopite along with commonly associated amphibole can replace garnet (Fig. 3d) or these two phases occur in apparent equilibrium with garnet in its marginal part (Fig. 3e). Locally, phlogopite also forms tiny flakes in the matrix in the vicinity of garnet. Discrete flakes of barian phlogopite associated with chromite and garnet II were rarely observed in the rim part of garnet in harzburgite 322 (Fig. 3f).

Barian mica and its composition

The chemical composition of barian mica in the MSI from lherzolites varies, with a Ba content of 0.24–0.67 apfu in the I-site and a X_{Mg} ratio of ~0.85 to 0.95, thus ranging from Ba-rich phlogopite to kinoshitalite. By contrast, barian mica in the MSI in harzburgites exhibits a more uniform and high Ba content in the I-site (~0.35 to 0.58 apfu Ba) and a high X_{Mg} ratio of ~0.90 to 0.93 (Table 2; Fig. 5).

Beside Ba, the interlayer site of barian micas from the studied MSI is filled by K (0.21–0.64 apfu), minor Na (0.1–1.2 wt% Na_2O) and Sr (≤0.38 wt% SrO), and its occupancy is close to 1 (Table 2). The tetrahedral site is completely filled by Si and Al cations (high ^{IV}Al = 1.38–1.78 apfu; Fig. 5a). The octahedral sites display high Mg (1.83–2.55 apfu), minor Fe (0.11–0.36 apfu), Cr (0.03–0.22 apfu Cr in lherzolite; 0.23–0.50 apfu Cr in harzburgite) and ^{VI}Al (0.08–0.35 apfu), low Ti (0–2.80 wt% TiO_2; 0–0.16 apfu Ti), and traces of Ni (0.1–0.3 wt%) (Table 2; Fig. 5c, d, h). The calculated structural formulae indicate vacancies in the octahedral sites (0.11–0.32 pfu; Table 2; Fig. 5j). All micas are characterized by relative enrichment of Cl over F (0.04–0.34 apfu Cl, ≤0.03 apfu F; Table 2; Fig. 5e–g). We assume that the rest of the A-site is occupied by OH and that there is no significant O^{2-} because analytical data (no high Ti as an indicator of oxy-micas, no trend to high oxide totals) do not provide any evidence for possible oxy-hydroxy exchange.

Phlogopite at the garnet rims in both the lherzolites and harzburgite differs in chemical composition from that in the MSI, containing less Ba (0.02–0.20 apfu in lherzolites; 0.22–0.27 apfu in harzbugite), ^{IV}Al (1.19–1.38 apfu), Cr (0.03–0.09 apfu Cr in lherzolite; ~ 0.17 apfu Cr in harzburgite), Cl (<0.10 apfu), and more Si (2.62–2.81 apfu), F (0.02–0.07 apfu) and having a uniform, high X_{Mg} ratio of ~0.92 to 0.94 (Table 2; Fig. 5).

Besides Ba-rich phlogopite to kinoshitalite, no other common mineral in the MSI is a significant carrier of barium apart from the rare norsethite [$BaMg(CO_3)_2$] (Tables 1, 3). Amphibole in the MSI typically contains trace amounts of Ba (0.13–0.69 wt% BaO; Table 3).

Discussion

Ba-rich mica makes part of the MSI mineral assemblage enclosed in pyrope-rich garnet of the peak mineral assemblage in garnet peridotite. Such MSI represent trapped fluids (e.g. Frezzotti and Ferrando 2015) and their major and trace element composition has been used to characterize their source. However, the fine-grained and polycrystalline character of the MSI requires application of advanced and time-consuming techniques such as EDS-based bulk analysis of MSI area using SEM rastering, laser ablation ICP–MS of MSI, or experimental re-homogenisation of the MSI followed by electron, ion microprobe or LA ICP–MS analysis (e.g. Halter et al. 2002; Pettke et al. 2004; Malaspina et al. 2006; Rollinson et al. 2018). We demonstrate below that the study of the chemical composition of barian mica alone using a generally accessible technique (EMP) and the knowledge of operating substitution mechanisms can provide information on the composition of the mica crystallization medium and make inferences regarding their source. Phlogopite is a common mafic mineral of MSI from UHP garnet peridotites, although its chemical composition and/or contents of elements such as Ba, Sr, Cl and F have not been always determined (e.g. van Roermund et al. 2002; Zaccarini et al. 2004; Malaspina et al. 2006; Naemura et al. 2008; Vrijmoed et al. 2008).

Substitution trends in barian mica

All textural types of barian mica in studied peridotites belong to trioctahedral micas and they can be described as a solid solution of phlogopite $KMg_3(Si_3Al)O_{10}(OH)_2$, kinoshitalite $BaMg_3(Al_2Si_2)O_{10}(OH)_2$ and ferrokinoshitalite $BaFe_3(Al_2Si_2)O_{10}(OH)_2$. The observed relationships between Ba and ^{IV}Al as well as between K + Na + Si and Ba + Ca + ^{IV}Al (Fig. 5a, b) correspond to the exchange vector

$$Ba\ ^{IV}AlK_{-1}Si_{-1} \quad (1)$$

which is the most common case in trioctahedral micas (e.g. Mansker et al. 1979; Dasgupta et al. 1989). This trend follows the evolution from phlogopite to kinoshitalite or from annite to ferrokinoshitalite.

Moreover, a negative correlation between Ba and Mg (with the slope of regression line ~ − 1) and positive one between Ba and Fe (the slope of regression line ~ 1), exhibited particularly by mica from MSI in lherzolites (Fig. 5c, d) indicate a more complex substitution trend

$$BaFe\ ^{IV}AlK_{-1}Mg_{-1}Si_{-1} \quad (2)$$

involving a decrease of phlogopite and an increase of ferrokinoshitalite along with kinoshitalite end-members rather than a simple coupled substitution (1).

An additional substitution trend observed in mica is that of Cl for OH. There is an obvious positive correlation between Cl, Ba and Fe (with the slope of regression line ~ 1) and a negative one between Cl and Mg (Fig. 5e–g) exhibited by the majority of barian micas, except Cl-poor phlogopite associated with amphibole close to garnet rim in lherzolite. Taking into account the relationships expressed by vectors (1), (2) and the Cl–OH exchange, the final coupled substitution vector involving Ba in the I-site and describing well observed chemical variability can be expressed as

$$BaFe\ ^{IV}AlClK_{-1}Mg_{-1}Si_{-1}(OH)_{-1}. \quad (3)$$

Table 2 Representative chemical composition of barian mica in MSI (analyses 1–9) and other textural types in peridotites (analyses 10–12)

	1	2	3	4	5	6	7	8	9	10	11	12
Rock	lherz.	lherz.	lherz.	lherz.	lherz.	lherz.	harzb.	harzb.	harzb.	lherz.	lherz.	harzb.
Sample	332	332	313	313	282	282	322	322	276	332	313	322
SiO_2	27.52	29.24	30.36	34.59	31.08	32.02	29.29	29.85	30.27	38.24	39.66	35.57
TiO_2	bdl	bdl	1.98	0.78	1.55	0.79	0.22	0.13	0.19	1.31	1.50	0.70
Al_2O_3	20.10	19.68	18.96	20.21	18.50	18.93	20.99	20.54	19.42	17.06	15.96	16.80
Cr_2O_3	3.42	2.66	0.98	1.13	0.73	0.98	4.77	6.83	4.21	0.99	0.87	2.81
V_2O_3	0.07	0.04	0.05	bdl	bdl	0.05	0.09	0.09	0.06	bdl	0.05	0.10
FeO	5.24	4.00	4.14	1.85	3.73	2.48	2.56	2.51	2.51	2.96	2.75	2.34
MnO	bdl	bdl	bdl	bdl	0.02	bdl	bdl	bdl	0.03	bdl	bdl	bdl
MgO	16.43	18.38	19.57	21.90	20.35	21.53	16.38	15.62	17.05	23.86	23.85	21.96
NiO	0.11	0.15	bdl	0.11	0.06	0.12	0.08	0.10	0.16	0.21	0.22	0.15
ZnO	0.06	0.11	bdl	bdl	0.07	bdl	bdl	bdl	bdl	bdl	bdl	bdl
BaO	19.09	18.54	14.64	8.60	14.11	11.44	18.44	18.32	17.83	3.46	0.77	7.66
SrO	bdl	bdl	bdl	bdl	bdl	bdl	0.18	0.21	0.10	bdl	bdl	bdl
CaO	0.58	0.52	0.63	0.43	0.72	0.19	0.12	0.36	0.32	0.02	0.03	0.05
K_2O	2.05	2.69	3.89	6.32	3.26	4.92	2.93	3.00	2.99	7.85	9.15	7.78
Na_2O	0.46	0.59	0.65	0.88	0.95	0.94	0.45	0.19	0.29	1.06	0.84	0.19
F	bdl	bdl	0.10	bdl	bdl	0.05	bdl	bdl	bdl	0.20	0.31	0.11
Cl	2.39	1.94	1.13	0.44	1.26	0.86	1.14	1.27	1.58	0.07	0.06	0.76
F, Cl = –O	0.54	0.44	0.30	0.10	0.28	0.21	0.26	0.29	0.36	0.10	0.15	0.22
H_2O*	3.03	3.26	3.50	3.99	3.52	3.66	3.48	3.49	3.35	4.13	4.09	3.80
Total	98.68	100.30	99.61	100.90	98.92	98.22	100.25	101.53	99.13	101.25	99.95	100.19
T-site												
Si^{4+}	2.266	2.339	2.375	2.529	2.426	2.465	2.331	2.351	2.422	2.707	2.798	2.636
Al^{3+}	1.734	1.661	1.625	1.471	1.574	1.535	1.669	1.649	1.578	1.293	1.202	1.364
Subtotal	4.000	4.000	4.000	4.000	4.000	4.000	4.000	4.000	4.000	4.000	4.000	4.000
M-site												
Al^{3+}	0.217	0.194	0.124	0.271	0.128	0.182	0.301	0.258	0.254	0.130	0.124	0.104
Ti^{4+}	0.000	0.000	0.117	0.043	0.091	0.045	0.013	0.008	0.012	0.069	0.080	0.039
Cr^{3+}	0.222	0.168	0.060	0.065	0.045	0.060	0.300	0.425	0.266	0.055	0.049	0.165
V^{3+}	0.005	0.003	0.003	0.001	0.000	0.003	0.006	0.005	0.004	0.001	0.003	0.006
Fe^{2+}	0.361	0.267	0.271	0.113	0.244	0.159	0.171	0.165	0.168	0.175	0.162	0.145
Mn^{2+}	0.000	0.000	0.000	0.000	0.001	0.000	0.000	0.000	0.002	0.000	0.000	0.000
Mg^{2+}	2.017	2.191	2.283	2.387	2.368	2.471	1.944	1.834	2.033	2.517	2.508	2.427
Ni^{2+}	0.007	0.010	0.000	0.006	0.004	0.007	0.005	0.006	0.010	0.012	0.012	0.009
Zn^{2+}	0.004	0.007	0.000	0.000	0.004	0.000	0.000	0.000	0.000	0.000	0.000	0.000
Subtotal	2.834	2.840	2.858	2.886	2.885	2.928	2.740	2.701	2.749	2.959	2.938	2.895
I-site												
Ba^{2+}	0.616	0.581	0.449	0.246	0.431	0.345	0.575	0.565	0.559	0.096	0.021	0.223
Sr^{2+}	0.000	0.000	0.000	0.000	0.000	0.000	0.008	0.010	0.005	0.000	0.000	0.000
Ca^{2+}	0.051	0.045	0.052	0.034	0.060	0.016	0.010	0.031	0.027	0.002	0.002	0.004
K^+	0.215	0.275	0.388	0.589	0.325	0.483	0.298	0.302	0.305	0.709	0.824	0.735
Na^+	0.073	0.091	0.098	0.125	0.143	0.140	0.070	0.030	0.045	0.146	0.115	0.027
Subtotal	0.955	0.991	0.987	0.995	0.959	0.983	0.961	0.937	0.941	0.953	0.965	0.991
A-site												
F^-	0.000	0.000	0.024	0.000	0.000	0.011	0.000	0.000	0.000	0.044	0.070	0.026
Cl^-	0.334	0.263	0.149	0.055	0.167	0.112	0.154	0.169	0.214	0.008	0.007	0.095
OH^-	1.666	1.737	1.826	1.945	1.833	1.877	1.846	1.831	1.786	1.948	1.923	1.878
Subtotal	2.000	2.000	2.000	2.000	2.000	2.000	2.000	2.000	2.000	2.000	2.000	2.000
X_{Mg}	0.848	0.891	0.894	0.955	0.907	0.939	0.919	0.917	0.924	0.935	0.939	0.944

Crystal-chemical formulas of barian mica were calculated on the basis of twelve O + Cl + F atoms

All Fe is reported as Fe^{2+}. H_2O* is calculated by stoichiometry

Lherz. lherzolite, *harzb*. harzburgite

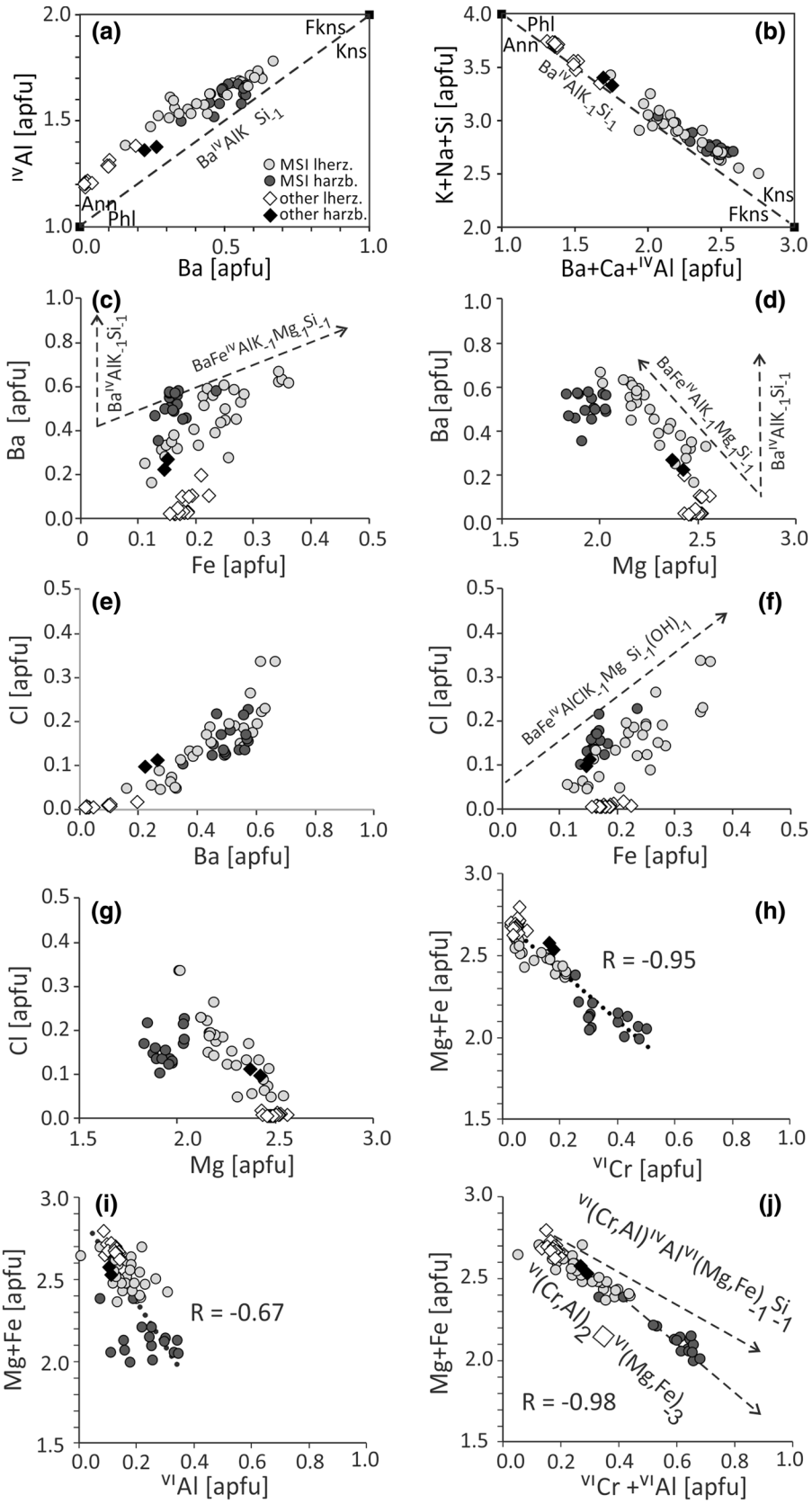

Fig. 5 Compositional variation and substitution trends in barian mica in MSI from lherzolite (light grey circle) and harzburgite (dark grey circle), also showing the composition of other barian micas from the rocks (lherzolite—white diamond; harzburgite—black diamond); **a** ^{IV}Al vs Ba; **b** K + Na + Si vs Ba + Ca + ^{IV}Al; **c** Ba vs Fe; **d** Ba vs Mg; **e** Cl vs Ba; **f** Cl vs Fe; **g** Cl vs Mg; **h** Mg + Fe vs Cr; **i** Mg + Fe vs ^{VI}Al; **j** Mg + Fe vs Cr + ^{VI}Al; all values in apfu. The dotted lines result from the least-squares fit, *R* is a correlation coefficient, and the dashed lines are substitution vectors. *Phl* phlogopite, *Ann* annite, *Kns* kinoshitalite, *Fkns* ferrokinoshitalite, *lherz.* lherzolite, *harzb*. harzburgite

Table 3 Average chemical composition (μ) and standard deviation (±2σ) of representative minerals from MSI; n = number of analytical points

Rock	lherz.+harzb.		lherz.+harzb.		lherz.+harzb.		lherzolite		harzburgite		lherzolite		harzburgite		harzburgite	
Mineral	Nrs		Dol		Mgs		Hbl		Hbl		Cpx		Cpx		Opx	
n	3		8		7		23		5		4		5		4	
Oxide/wt.%	μ	±2σ	μ	±2σ	μ	±2σ	μ	±2σ	μ	±2σ	μ	±2σ	μ	±2σ	μ	±2σ
SiO_2	0.63	0.00	0.28	0.16	0.44	0.37	43.87	1.96	45.67	2.96	54.27	0.49	53.16	3.20	57.04	2.01
TiO_2	0.00	0.00	0.01	0.02	0.00	0.00	0.32	0.40	0.00	0.00	0.06	0.15	0.01	0.05	0.01	0.04
Al_2O_3	0.42	0.17	0.04	0.08	0.06	0.10	16.91	1.46	13.06	2.31	11.56	5.11	6.86	2.81	2.22	1.26
Cr_2O_3	0.23	0.17	0.15	0.15	0.12	0.07	1.52	0.89	3.18	0.77	2.01	1.04	3.29	1.14	0.88	0.40
FeO	1.12	0.11	2.13	1.08	4.63	3.60	2.34	0.88	1.61	0.10	2.13	1.32	1.89	0.95	3.41	0.60
MnO	0.00	0.00	0.18	0.13	0.21	0.19	0.04	0.08	0.00	0.00	0.06	0.08	0.09	0.10	0.04	0.07
MgO	16.99	1.46	22.06	2.90	44.36	2.06	17.41	0.92	18.58	1.04	9.85	2.89	13.32	3.65	34.86	1.37
NiO	0.00	0.00	0.00	0.00	0.02	0.06	0.04	0.09	0.03	0.12	0.00	0.00	0.02	0.07	0.01	0.04
ZnO	0.05	0.10	0.02	0.06	0.00	0.00	0.02	0.08	0.02	0.07	0.00	0.00	0.02	0.06	0.04	0.08
BaO	**52.28**	2.48	**0.10**	0.07	**0.06**	0.15	**0.45**	0.34	**0.36**	0.09	**0.04**	0.15	**0.04**	0.10	**0.11**	0.32
SrO	0.16	0.11	0.34	0.56	0.04	0.05	0.03	0.15	0.08	0.16	0.00	0.00	0.00	0.00	0.00	0.00
CaO	1.99	2.93	31.11	2.98	1.06	0.55	10.13	2.20	12.24	0.50	13.69	5.50	17.12	3.49	0.86	1.03
K_2O	0.03	0.05	0.01	0.03	0.00	0.00	0.36	0.23	0.39	0.08	0.01	0.04	0.00	0.00	0.03	0.11
Na_2O	0.04	0.09	0.04	0.08	0.00	0.00	4.47	1.15	2.79	0.14	6.53	2.53	4.24	1.63	0.08	0.10
F	0.00	0.00	0.00	0.00	0.00	0.00	0.12	0.05	0.12	0.03	0.00	0.00	0.00	0.00	0.00	0.00
Cl	0.00	0.00	0.00	0.00	0.00	0.00	0.37	0.42	0.27	0.11	0.00	0.00	0.00	0.00	0.00	0.00
Total	74.42		56.65		51.07		98.46		98.59		100.41		100.27		99.75	

Average Ba contents in minerals from MSI are in bold

Note that traces of Ba in dolomite, magnesite or pyroxenes may be due to overlapping excitation volume with adjacent kinoshitalite or by a secondary fluorescence of Ba in kinoshitalite near the beam impact spot. For abbreviations of minerals see Table 1

Lherz. lherzolite, *harzb*. harzburgite

In addition to the chemical variability involving the incorporation of Ba into the mica structure following the trend (3), a minor amount of Cr and ^{VI}Al enters octahedral sites instead of Mg (Fe) (Fig. 5h, i). The observed relationships suggest the substitution trend

$$^{VI}(Cr, Al)_2\square\ ^{VI}(Mg, Fe)_{-3} \quad (4)$$

towards chromphyllite and muscovite rather than the entrance of Al via eastonite/siderophyllite end-member (Fig. 5j). This trend is confirmed by a simultaneous increase of vacancy (0.13–0.30 pfu) along with Cr and ^{VI}Al in octahedral sites. High Cr contents are not characteristic of trioctahedral but Ba-rich dioctahedral micas, where substitution of Cr^{3+} instead of ^{VI}Al results in the expansion of the octahedral sheet and enlarges the interlayer site (e.g. Tracy 1991; Pan and Fleet 1991).

Factors controlling the chemical composition of barian mica and the role of fluids

The chemical composition of the mica-forming medium represents the first-order control on barian mica composition. Our data show that apart from the host environment, i.e. the host phase (garnet) and the host rock (peridotite/harzburgite), an external source is needed to account for additional elements, which—as will be demonstrated below—is the subducting crustal slab. Nevertheless, the barian mica composition is also controlled by its crystal structure. In many cases, both the chemical composition of the source material and structural factors work together.

The average X_{Mg} of barian mica in the rock samples studied is similar to their host-rock X_{Mg} (Fig. 6a) and slightly higher than the X_{Mg} of the host garnet (0.79–0.84 in lherzolite and 0.81–0.85 in harzburgite), reflecting the composition of the host rock/phase, thus suggesting an internal source of Mg and Fe. Along with relatively high Al contents, the Cr abundances in barian mica are comparable to the composition of the host garnet, being much lower in the host rocks (0.31–0.40 wt% Cr_2O_3; 1.3–3.9 wt% Al_2O_3; data from Medaris et al. 2015; Fig. 6b). Textural relationships, i.e. barian mica occurrence at the margin of the MSI in harzburgites (Fig. 4e), as well as association of phlogopite with the garnet rim (Fig. 2d–f) suggest, that garnet also represents the main source of Al, although some Al might have introduced from an external source by supercritical fluids due do its high solubility in such fluids (e.g. Manning 2004; Hermann et al. 2006).

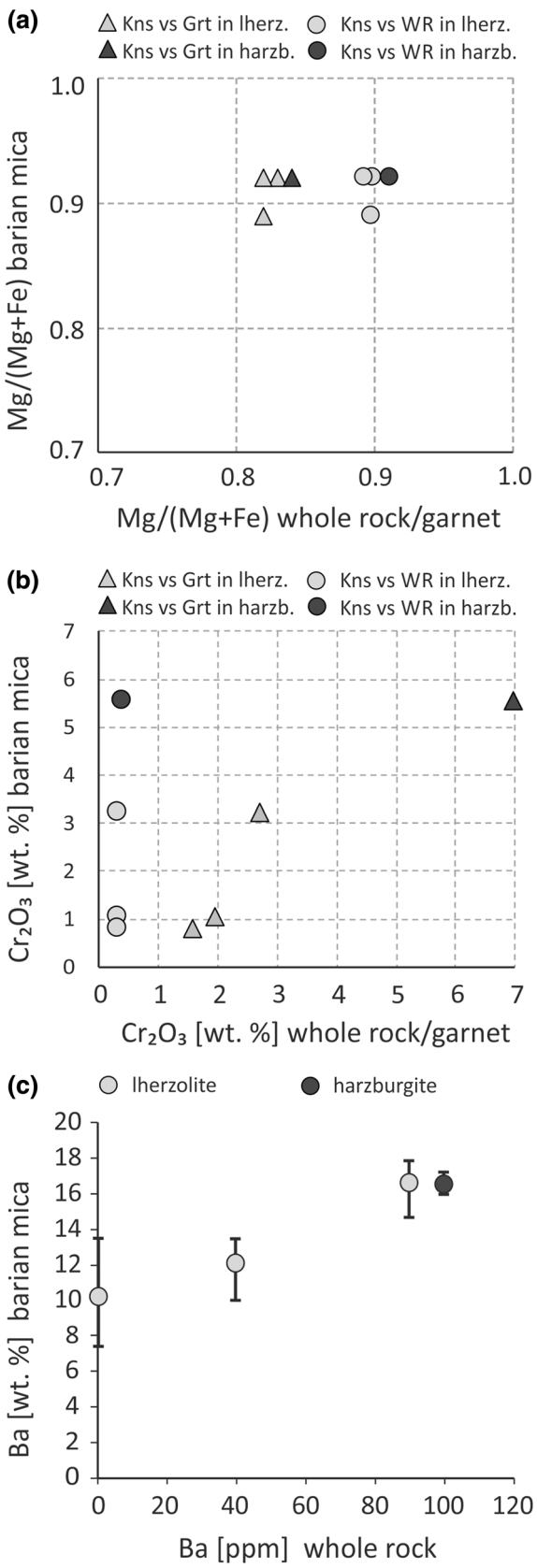

Fig. 6 Relationships between the chemical composition of barian mica in MSI and their host environment (peridotite and garnet); **a** average Mg/(Mg+Fe) in barian mica vs Mg/(Mg+Fe) in whole rock (circles) and garnet (triangles); **b** average Cr_2O_3 in barian mica vs Cr_2O_3 in whole rock (circles) and garnet (triangles); **c** variation of Ba content in barian mica (average, minimum and maximum contents) vs. whole rock Ba concentrations. Light grey colour—lherzolite (lherz.); dark grey colour—harzburgite (harzb.)

Although the Ba abundances in the host garnet peridotites are low (< 0.3 to 100 ppm), they vary from values typical of the primitive mantle to those of a Ba-enriched mantle (Palme and O'Neill 2014). Barium almost exclusively occurs in the phases of MSI, predominantly barian mica, as is also documented by a positive correlation of the Ba content in the mica, the mica abundance in the MSI, and the Ba content in the host rock (Table 1; Fig. 6c). Barium and other LILE concentrate in magmatic and (meta)sedimentary crustal rocks, which can contain Ba on the order of thousands of ppm (e.g. Taylor and McLennan 1985; Edgar 1992; Seifert and Kampf 1994; Massonne et al. 2013). This suggests an external source of Ba (± K, ± Sr, i.e. LILE) introduced into the mantle rocks by crustal-derived fluids during the subduction of the continental crust. Similarly, high Cl together with a high Cl/*F* ratio reflects the high f_{Cl} and relatively low f_F in the subduction-zone fluids. Apart from the high Cl abundances in kinoshitalite, the presence of chlorapatite and minor Cl in amphibole, other Cl- bearing phases are absent in the MSI, although chlorides (halite, sylvite) have been rarely described in the MSI from other UHP terranes (e.g. Philippot et al. 1995). The presence of barian mica rich in Cl in the MSI thus requires a mass transfer of elements (K, Ba, Sr, Cl) from the subducting slab to the overlying mantle wedge. In summary, the major and minor element budget of barian mica in the MSI, along with the presence of Th, U and LREE-rich phases, is compatible with the composition of subduction-related fluids (e.g. Spandler and Pirard 2013; Keppler 2017).

Aqueous fluids produced during the dehydration of water-rich minerals of the subducting plate facilitate water-saturated melting at the top of the slab (e.g. Hermann and Rubatto 2009, 2014; Spandler and Pirard 2013). At ultrahigh pressures of the deep subduction relevant to our study, however, complete miscibility between the aqueous fluid and silicate melt occurs above the second critical endpoint and supercritical fluids are stable. Such supercritical solute-rich aqueous fluids to hydrous melts (rich in the volatiles H, C, Cl, S) can carry high amounts of alkalies, LILE (Ba, Cs, Sr, K), Th, U and LREE due to their high solubility, which can be enhanced by the formation of complex aluminosilicate-based polymers (e.g. Manning 2004; Hermann et al. 2006; Spandler and Pirard 2013; Zheng and Hermann 2014). At UHP–UHT conditions reflected by our diamond-bearing metasediments (c. 1100 °C and 4.5 GPa) located above the

second critical point in pelitic systems (~3 GPa; Hermann et al. 2006), the produced supercritical fluids transporting the elements into the overlying mantle wedge had the properties of a hydrous melt.

The local crystal structure control on the barian mica composition is demonstrated by variable Ba contents positively correlating with Fe in mica from lherzolites (Fig. 5c). The entrance of Fe^{2+} instead of Mg enlarges the octahedral site and facilitates the incorporation of a large Ba cation in the I-site. The high Cl content in barian mica reflects its crystallization from a fluid phase with high f_{Cl}. In addition, the variability in the Cl content and its positive and negative correlation with Fe and Mg, respectively (Fig. 5f,g), reflect the structural control of Cl-OH substitution in barian mica. Similar relationships have been reported between OH-phlogopite and Cl-annite (e.g. Munoz and Swenson 1981; Volfinger et al. 1985). The dimension of the A-site is mainly controlled by the α angle, the decrease of which enables replacement of OH^- by larger Cl^-. The Fe^{2+}–Mg^{2+} exchange in the phlogopite–annite solid solution results in an increase in the size of the octahedra and a decrease in the α angle (Volfinger et al. 1985).

Specific chemical composition of barian mica related to a subduction environment

The barian mica from the MSI hosted by garnet in garnet peridotites exhibit a distinct chemical composition (very high Mg#, high Si + Al; very low contents of Mn, Zn, Ti and F; enrichment in Cr and Cl) compared to other localities worldwide (Figs. 7, 8; and references therein).

The barium content in studied mica from MSI is rather high (up to 20 wt% BaO and 0.67 apfu Ba; Fig. 7a), whereas sporadic phlogopite grains close to the garnet margin or at its rim contain less barium (0.75–8.96 wt% BaO). The high Ba content corresponding to the kinoshitalite/ferrokinoshitalite field characteristic of our MSI is typical of metamorphosed Mn, Fe deposits and marbles, being rare in mica from a magmatic environment. A high Ba content in mica from subduction-related settings was documented in Cl-rich ferrokinoshitalite (16–24 wt% BaO) from the metasomatised contact domain between supra-subduction peridotite and metasediment (Tumiati et al. 2007). Phlogopite with minor Ba contents has also been reported in the matrix and in kelyphites around garnet in metasomatised peridotites from the Alps and Bohemian Massif (0.2–4.1 wt% BaO; Zanetti et al. 1999; Naemura et al. 2009; Medaris et al. 2015). The available data for mica in the MSI in other terranes (0.1–9.0 wt% BaO—Zaccarini et al. 2004; Malaspina et al. 2006; Naemura et al. 2008) plot much below the kinoshitalite field, although the Ba contents in mica in MSI is always higher than that of the barian mica in the matrix (Fig. 7a). However, low contents of K and a significant deficit of cations in the I-site in published phlogopite analyses in the MSI from some other mantle-derived ultramafic rocks (van Roermund et al. 2002; Malaspina et al. 2015) and occurrence of Ba–Mg carbonates associated with phlogopite in MSI (van Roermund et al. 2002) could indicate a barium enrichment of these phlogopites as well.

As for subduction-related crustal rocks, Ba-rich oxyannite with up to 13.4 wt% BaO has recently been described in the calcic gneisses associated with the UHP metasediments of the Seve Nappe Complex (Majka et al. 2015). Moreover, Ba-rich phengitic muscovite has been reported in subducted metasediments, a subduction-related serpentinite mélange and eclogites of various collisional belts (up to 14.5 wt% BaO; Harlow 1995; Sorensen et al. 1997; Massonne and Burchard 2000; Bocchio 2007; Massonne et al. 2013).

The very high Mg# of the studied barian mica is comparable to some micas from metasomatised mafic and ultramafic rocks, metamorphosed Mn deposits, marbles and kimberlites (Fig. 7). The high Si + Al content (significantly > 4 apfu) due to high Al (both ^{IV}Al and ^{VI}Al) (Fig. 7b) is exhibited by barian micas from metasomatised high-grade ultramafic rocks, mafic rocks and calcic gneiss. The high Cr content (up to 0.43 apfu) is unique for trioctahedral micas and reflects the mantle protolith. Ba-rich phlogopites from metasomatised peridotites, mainly those reported from the MSI hosted in spinel (Zaccarini et al. 2004; Naemura et al. 2008), also contain minor Cr (Fig. 8a). On the other hand, Mn (± Zn) and Ti are low in the studied mica, similar to other metasomatised orogenic peridotites, and in contrast to barian micas from Mn, Fe deposits, skarns and marbles, magmatic rocks, metasomatised calcic gneisses or mafic granulites (Fig. 8b).

Studied micas have elevated Cl abundances in line with barian mica in metasomatised Ulten peridotites (Tumiati et al. 2007), barian mica in noritic granulite (Kullerud 1995), and phlogopite in MSI from eclogite slices (Faryad et al. 2013). The chlorine contents in mica from our samples vary; however, their fluorine contents are always low, in contrast to the majority of other occurrences (Fig. 8c). This suggests that chlorine enrichment, and fluorine depletion, is a significant feature of trioctahedral mica from a subduction-related environment including a supra-subduction lithospheric mantle.

Our study and comparison with other barian mica occurrences worldwide (Figs. 7, 8) show that barium-rich mica present in SiO_2-poor host rocks, such as UHP peridotites, serpentinites, or eclogites, represents a tracer of a subduction environment.

Potential Ba sources in the subducted Saxothuringian crust

Phengite-bearing metasediments of the subducted Saxothuringian crust represent a potential Ba (+ other LILE, namely

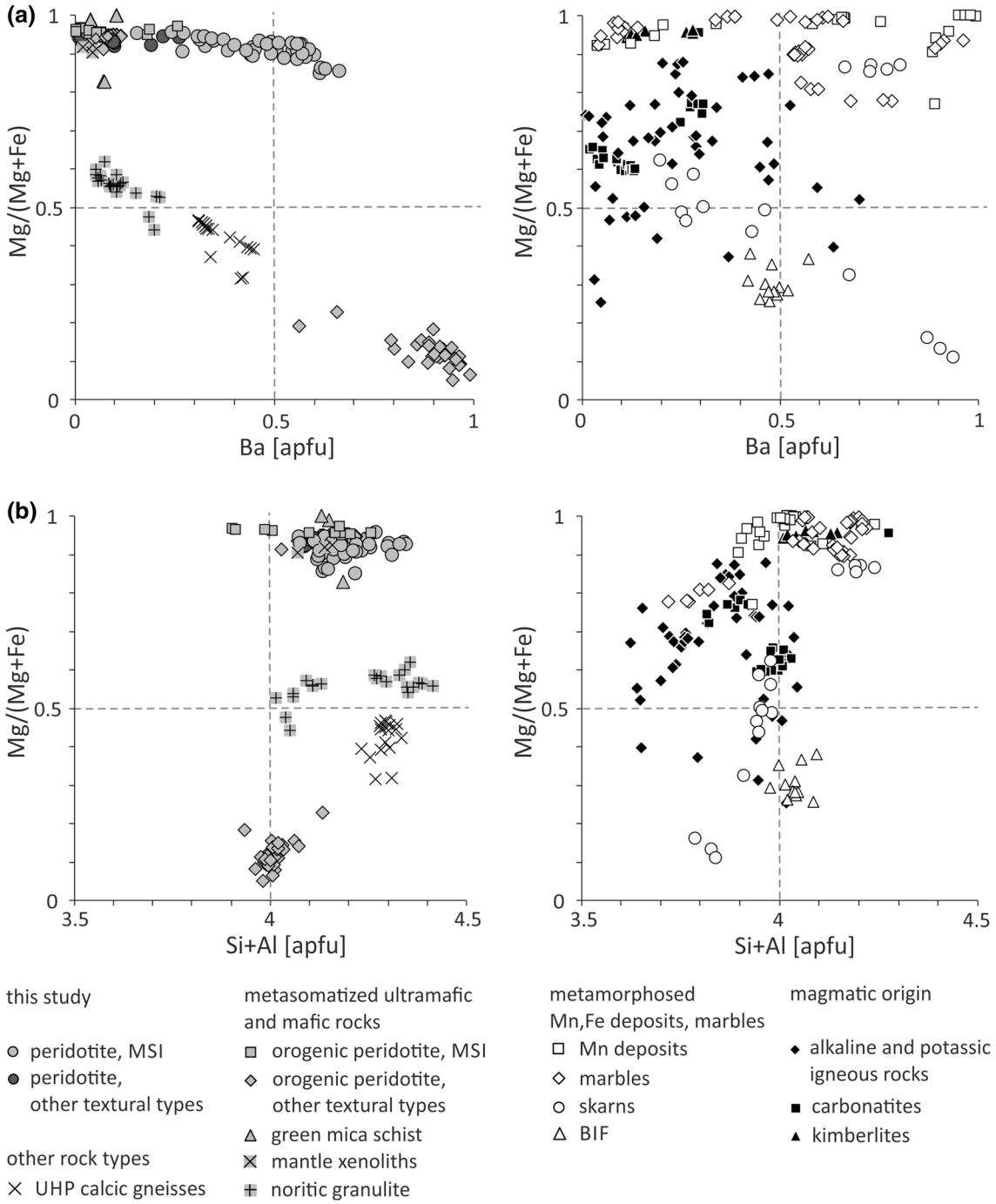

Fig. 7 Comparison of the compositional variation of major elements in trioctahedral barian micas from this work (light grey circles—mica from MSI in peridotites; dark grey circles—other textural types in peridotites) and worldwide occurrences; **a** Mg/(Mg + Fe) vs Ba; **b** Mg/(Mg + Fe) vs Si + Al. Magmatic barian mica (black symbols) from alkaline and potassic igneous rocks (Mansker et al. 1979; Edgar 1992; Zhang et al. 1993; Seifert and Kampf 1994; Shaw and Penczak 1996; Greenwood 1998; Kogarko et al. 2005; Manuella et al. 2012), carbonatites (Gaspar and Wyllie 1982; Solovova et al. 2009) and kimberlites (Zurevinski and Mitchell 2011). Barian mica from regionally and contact metamorphosed Mn, Fe deposits (Yoshii and Maeda 1975; Dasgupta et al. 1989; Frimmel et al. 1995; Guggenheim and Frimmel 1999; Gnos and Armbruster 2000), calc-silicate rocks (Tracy 1991; Tracy and Beard 2003) and marbles (Solie and Su 1987; Bol et al. 1989; Tracy 1991; Tracy and Beard 2003; Doležalová et al. 2006; Houzar and Cícha 2016) (white symbols). Metasomatic barian mica from mafic–ultramafic rocks (grey symbols)—barian mica in matrix, kelyphites and shear zones in orogenic garnet peridotites (Zanetti et al. 1999; Tumiati at al. 2007; Naemura et al. 2009), barian mica from MSI in orogenic garnet peridotites (Zaccarini et al. 2004; Naemura et al. 2008, 2009), mantle xenoliths in alkali basalts (Ionov and Hofmann 1995), shear zone in mafic granulites (Kullerud 1995) and green mica schist (Pan and Fleet 1991). Metasomatic barian mica from UHP calcic gneisses (Majka et al. 2015). Values in apfu

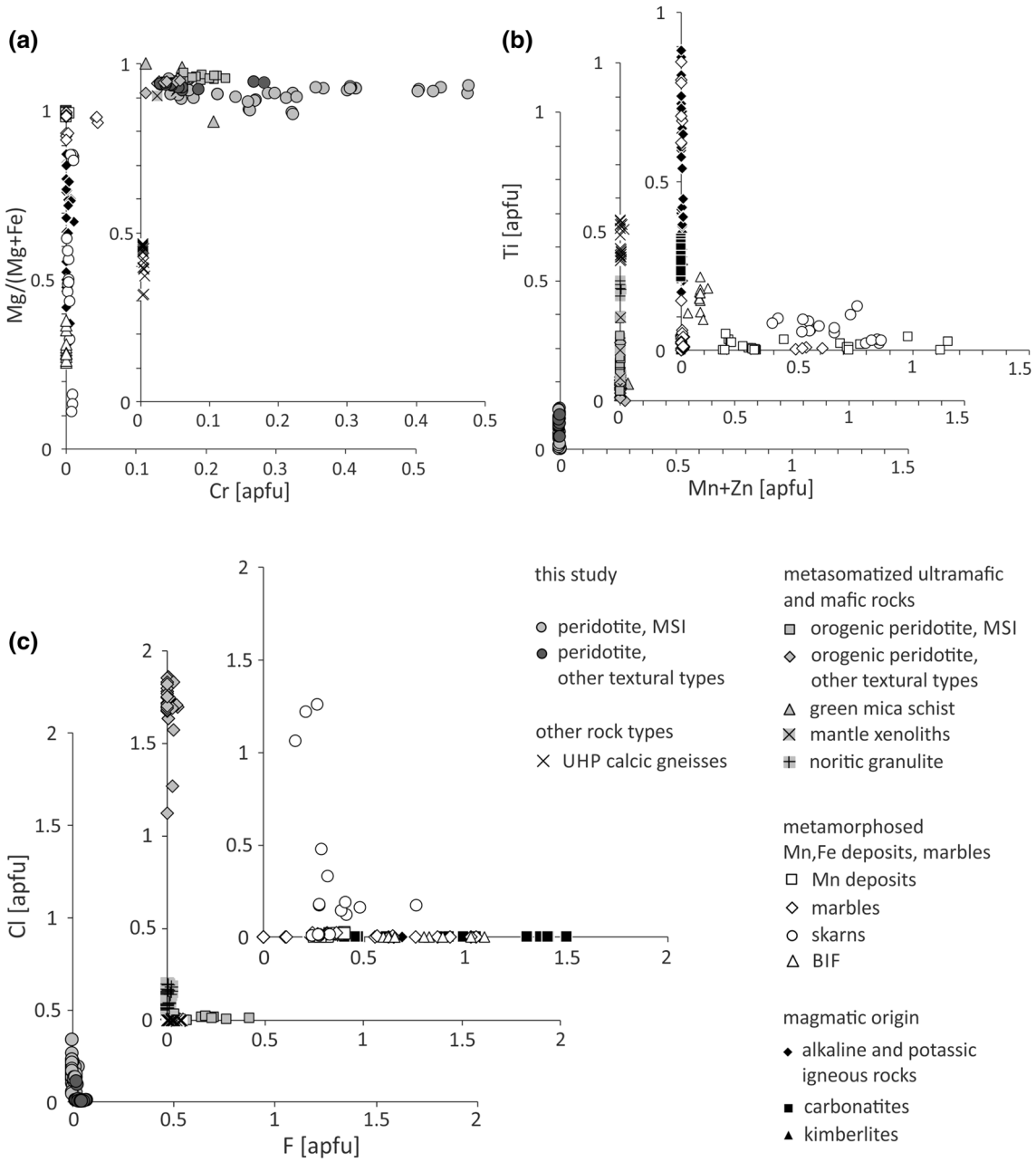

Fig. 8 Comparison of the variation of minor elements in trioctahedral barian micas from this work (light grey circles—mica from MSI in peridotites; dark grey circles—other textural types in peridotites) and worldwide occurrences; **a** Mg/(Mg + Fe) vs Cr; **b** Ti vs Mn + Zn; **c** A-site occupancy, Cl vs F (data sources similar to Fig. 5). Values in apfu

K and Sr) source for the Ba-rich mica formation in the MSI. The barium contents of the associated diamond-bearing metasediments (510–970 ppm, Kotková unpublished data) and high-pressure granulites (< 100 to 1480 ppm, Kotková 1993) as well as the UHP garnet–phengite gneiss from the Erzgebirge (100–1625 ppm, Behn et al. 2011) are rather low, less than half compared to the values reported for Ba-rich metasediments such as pelagic clays hosting Ba-rich phengite (Taylor and McLennan 1985; Massonne et al. 2013). However, barium is depleted in the UHT metasediments as melts form due to phengite breakdown and mediate Ba and other lithophile element transport into the overlying units (Hermann et al. 2006; Behn et al. 2011; Hermann and Rubatto 2014). Transfer of other slab-derived elements, LREE, P, Th and U is supported by the presence of monazite, Cl-apatite and thorianite/uraninite in the MSI. The presence of carbonates in the source is required for the formation of voluminous carbonates in the MSI, however, no such

rocks are exposed in the area. Ongoing research including the definition of the bulk chemical composition of the MSI and a determination of the C and O isotope composition of the MSI carbonates in-situ will further constrain the source rocks.

Multiphase solid inclusions in UHP rocks and mantle metasomatism

The polygonal or negative crystal shape of the studied MSI reflects their primary character (e.g. Frezzotti and Ferrando 2015). Although they represent fluids trapped in growing pyrope-rich garnet close to the estimated P–T peak (c. 1100 °C/4–5 GPa), the MSI textures indicating coeval crystallization of barian mica with the other phases reflect a (re)crystallization of the homogeneous fluid phase during decompression. The coexistence of pargasite, dolomite and magnesite along with spinel suggests pressures below c. 1.8–2 GPa and a still very high temperature (Schmädicke and Evans 1997; Tumiati et al. 2013; Mandler and Grove 2016 and references therein).

Our MSI are comparable to those occurring in the minerals of the peak assemblages of the UHP rocks of both crustal and mantle origin: gneisses and eclogites, as well as garnet pyroxenites and garnet peridotites. These are interpreted as crystallised supercritical fluids or hydrous melts, and their bulk trace element composition provides evidence for mantle metasomatism by liquids derived from a subducting continental slab (e.g. Malaspina et al. 2006, 2009; Frezzotti and Ferrando 2015).

The mineral proportions in the studied MSI reflect a variable degree of cryptic metasomatism in individual samples indicated by bulk rock chemical data (Medaris et al. 2015). The predominance of amphibole and the low modal amount of barian mica (i.e. relatively low bulk LILE content) in MSI is compatible with the primitive character of the samples 282 and 313, whereas the more enriched samples (lherzolite 332 and harzburgites) contain MSI with a higher modal amount of barian mica and common monazite reflecting relatively stronger LILE and LREE metasomatism (Table 1). In addition, the carbonate content in the MSI positively correlates with the degree of cryptic metasomatism.

Apart from the MSI, the metasomatism in our samples is only indicated by sporadic formation of barian phlogopite (± amphibole/±garnet II) associated with the garnet margin. By contrast, phlogopite-bearing MSI in other UHP terranes (Western Gneiss Region, Dabie-Sulu) occur in garnet peridotites, garnet websterites or garnet orthopyroxenites with evidence of modal metasomatism (phlogopite/Opx II/carbonate in the matrix) and refertilization (Carswell and van Roermund 2005; Vrijmoed et al. 2006; Malaspina et al. 2006, 2009; Scambelluri et al. 2010). Garnet peridotites from northern Bohemia thus represent a distinct example of apparently non-metasomatised mantle rocks, where metasomatism is recorded essentially by minute multiple solid inclusions in garnet (comp. also MSI-bearing garnet peridotites from Sulu; Malaspina et al. 2009).

Conclusions

We provide details on the composition and substitution trends of barian mica in mantle wedge peridotite from the northern Bohemian Massif. Phlogopite to kinoshitalite occurring in MSI hosted by pyrope-rich garnet represents an essential carrier of barium in these rocks with low bulk Ba contents (< 0.3 to 100 ppm). Trioctahedral barian mica has been typically described in crustal magmatic and metamorphosed rocks enriched in barium. Our study demonstrates that the enhanced Ba content in the rock does not represent a prerequisite for kinoshitalite formation.

In addition to Ba, mica in the MSI from the studied garnet peridotites is significantly enriched in Cr and Cl, and contains some Sr. The unusual chemical composition of the barian mica reflects metasomatism of the mantle material (high Mg, Mg#, Al, Cr and low Fe, Mn and Ti reflecting composition of bulk peridotite and/or host garnet) by crustal-derived subduction-zone fluids (source of Ba, K, Sr, Cl). UHP peridotites (and possibly other subduction-related SiO_2-poor rocks) may thus represent another typical, yet overlooked, environment that allows for the formation of Ba-rich phlogopite to kinoshitalite with such a specific chemistry.

Barian mica in MSI trapped in pyrope-rich garnet of the UHP–UHT peridotite assemblage is enriched in Ba relative to the metasomatic Ba-rich phlogopite in the peridotite matrix in this and other ultrahigh-pressure terranes. In addition, the modal amount of barian mica in the MSI correlates with the degree of subduction-related cryptic metasomatism as reflected by bulk chemical data for the host peridotites. Trioctahedral mica in the MSI thus represents a close snapshot of the composition of the crystallization medium with mixed crustal and mantle signatures in deep parts of the subduction zones.

Another significant implication of our study is the importance of determining the Ba contents in mica during EMP analyses even in rocks with low bulk Ba content. Similarly, the Cl abundance must be specified, also because its omission in analytical setup routines for mica or amphiboles along with the absence of chlorides in the mineral assemblage may be misinterpreted as a low activity of Cl in the source medium.

Our results show that a focused study of the MSI phases such as barian mica using a common and generally accessible technique (EMP) can significantly contribute to the characterization of the processes at convergent plate boundaries, and complement other much more demanding techniques.

Acknowledgements This research was financially supported by Czech Science Foundation Project 18-27454S. We wish to acknowledge the constructive comments and suggestions of J. Majka and of an anonymous reviewer, which significantly contributed to the final version of this paper. The authors thank Daniela Rubatto for editorial handling.

References

Behn MD, Kelemen PB, Hirth G, Hacker BR, Massonne H-J (2011) Diapirs as the source of the sediment signature in arc lavas. Nat Geosci 4:641–646. https://doi.org/10.1038/NGEO1214

Bocchio R (2007) Barium-rich phengite in eclogites from the Voltri Group (northwestern Italy). Per Mineral 76:155–167. https://doi.org/10.2451/2007PM0013

Bol LCGM, Bos A, Sauter PCC, Jansen JBH (1989) Barium-titanium-rich phlogopites in marbles from Rogaland, southwest Norway. Am Mineral 74:439–447

Carswell DA, van Roermund HLM (2005) On multi-phase mineral inclusions associated with microdiamond formation in mantle-derived peridotite lens at Bardane on Fiørtoft, west Norway. Eur J Mineral 17:31–42. https://doi.org/10.1127/0935-1221/2005/0017-0031

Dasgupta S, Chakraborti S, Sengupta P, Bhattacharya PK, Banerjee H, Fukuoka M (1989) Compositional characteristics of kinoshitalite from the Sausar Group, India. Am Mineral 74:200–202

Doležalová H, Houzar S, Losos Z, Škoda R (2006) Kinoshitalite with a high magnesium content in sulphide-rich marbles from the Rožná uranium deposit, Western Moravia, Czech Republic. N Jb Miner Abh 182:165–171. https://doi.org/10.1127/0077-7757/2006/0039

Edgar AD (1992) Barium-rich phlogopite and biotite from some Quaternary alkali mafic lavas, West Eifel, Germany. Eur J Mineral 4:321–330

Faryad SW, Jedlička R, Ettinger K (2013) Subduction of lithospheric upper mantle recorded by solid phase inclusions and compositional zoning in garnet: example from the Bohemian Massif. Gondwana Res 23:944–955. https://doi.org/10.1016/j.gr.2012.05.014

Frezzotti ML, Ferrando S (2015) The chemical behavior of fluids released during deep subduction based on fluid inclusions. Am Mineral 100:352–377. https://doi.org/10.2138/am-2015-4933

Frimmel HE, Hoffmann D, Watkins RT, Moore JM (1995) An Fe analogue of kinoshitalite from the Broken Hill Massie sulfide deposit in the Namaqualand Metamorphic Complex, South Africa. Am Mineral 80:833–840. https://doi.org/10.2138/am-1995-7-823

Gaspar JC, Wyllie PJ (1982) Barium phlogopite from the Jacupiranga carbonatite, Brazil. Am Mineral 67:997–1000

Gnos E, Armbruster T (2000) Kinoshitalite, $Ba(Mg)_3(Al_2Si_2)O_{10}(OH,F)_2$, a brittle mica from a manganese deposit in Oman: paragenesis and crystals chemistry. Am Mineral 85:242–250. https://doi.org/10.2138/am-2000-0125

Greenwood JC (1998) Barian–titanian micas from Ilha da Trindade, South Atlantic. Mineral Mag 62:687–695. https://doi.org/10.1180/002646198547918

Guggenheim S, Frimmel HE (1999) Ferrokinoshitalite, a new species of brittle mica from the Broken Hill mine, South Africa: structural and mineralogical characterization. Can Mineral 37:1445–1452

Haifler J, Kotková J (2016) UHP–UHT peak conditions and near-adiabatic exhumation path of diamond-bearing garnet-clinopyroxene rocks from the Eger Crystalline Complex, North Bohemian Massif. Lithos 248–251:366–381. https://doi.org/10.1016/j.lithos.2016.02.001

Halter WE, Pettke T, Heinrich CHA, Rothen-Rutishauser B (2002) Major to trace element analysis of melt inclusions by laser-ablation ICP–MS: methods of quantification. Chem Geol 183:63–86. https://doi.org/10.1016/S0009-2541(01)00372-2

Harlow GE (1995) Crystal chemistry of barian enrichment in micas from metasomatized inclusions in serpentinite, Motagua Fault Zone, Guatemala. Eur J Mineral 7:775–790. https://doi.org/10.1127/ejm/7/4/0775

Hermann J, Rubatto D (2009) Accessory phase control on the trace element signature of sediment melts in subduction zones. Chem Geol 265:512–526. https://doi.org/10.1016/j.chemgeo.2009.05.018

Hermann J, Rubatto D (2014) Subduction of continental crust to mantle depth: geochemistry of ultrahigh-pressure rocks. In: Holland HD, Turekian KK (eds) Treatise on geochemistry, 2nd edn. Elsevier, New York, pp 309–340. https://doi.org/10.1016/B978-0-08-095975-7.00309-0

Hermann J, Spandler C, Hack A, Korsakov AV (2006) Aqueous fluids and hydrous melts in high-pressure and ultra-high pressure rocks: implications for element transfer in subduction zones. Lithos 92:399–417. https://doi.org/10.1016/j.lithos.2006.03.055

Houzar S, Cícha J (2016) Chondrodite- and clinohumite-bearing marbles of the Podolsko Complex in Písek area and related F-rich Mg–Si–Ti–Ba–Zr mineral assemblage (Moldanubian Zone, Bohemian Massif). Bull mineral-petrolog Odd Nár. Muz (Praha) 24 1:33–45 **(in Czech)**

Ionov DA, Hofmann AW (1995) Nb–Ta-rich mantle amphiboles and micas: implications for subduction-related metasomatic trace element fractionations. Earth Planet Sci Lett 131:341–356. https://doi.org/10.1016/0012-821X(95)00037-D

Keppler H (2017) Fluids and trace element transport in subduction zones. Am Mineral 102:5–20. https://doi.org/10.2138/am-2017-5716

Kogarko LA, Uvarova YA, Sokolova E, Hawthorne FC, Ottolini L, Grice JD (2005) Oxykinoshitalite, a new species of mica from Fernando de Noronha island, Pernambuco, Brazil: occurrence and crystal structure. Can Mineral 43:1501–1510. https://doi.org/10.2113/gscanmin.43.5.1501

Kopecký L, Sattran V (1966) Buried occurrences of pyrope-peridotite and the structure of the crystalline basement in the extreme SW of the České středohoří Mts. Krystalinikum 4:65–86

Kopecký L, Paděra K (1974) Bänderung der ultramafi tischen Gesteine in der Bohrung T-7 Staré bei Trebenice (Nordböhmen), in Alexiev J et al. eds. Minerogenesis Bulgar Acad Sci Geol Inst Sofia 1974:161–169

Kotková J (1993) Tectonometamorphic history of lower crust in the Bohemian Massif-example of north Bohemian granulites. Czech Geol Surv Spec Pap 2:1–42

Kotková J, Janák M (2015) UHP kyanite eclogite associated with garnet peridotite and diamond-bearing granulite, northern Bohemian Massif. Lithos 226:255–264. https://doi.org/10.1016/j.lithos.2015.01.016

Kotková J, Kröner A, Todt W, Fiala J (1996) Zircon dating of North Bohemian granulites, Czech Republic: further evidence for the Lower Carboniferous high-pressure event in the Bohemian Massif. Geol Rundsch 85:154–161. https://doi.org/10.1007/BF00192073

Kotková J, O'Brien PJ, Ziemann MA (2011) Diamond and coesite discovered in Saxony-type granulite: solution to the Variscan garnet peridotite enigma. Geology 39:667–670. https://doi.org/10.1130/G31971.1

Kotková J, Whitehouse M, Schaltegger U, D'Abzac F-X (2016) The fate of zircon during UHT-UHP metamorphism: isotopic (U/Pb, δ18O, Hf) and trace element constraints. J Met Geol 34:719–739. https://doi.org/10.1111/jmg.12206

Kullerud K (1995) Chlorine, titanium and barium-rich biotites: factors controlling biotite composition and the implications for garnet-biotite geothermometry. Contrib Mineral Petrol 120:42–59. https://doi.org/10.1007/BF00311007

Liou JG, Ernst WG, Zhang RY, Tsujimori T, Jahn BM (2009) Ultrahigh-pressure minerals and metamorphic terranes—the view from China. J Asian Earth Sci 35:199–231. https://doi.org/10.1016/j.jseaes.2008.10.012

Majka J, Kruszewski Ł, Rosén Å, Klonowska I (2015) Ba-and Ti-enriched dark mica from the UHP metasediments of the Seve Nappe Complex, Swedish Caledonides. Mineralogia 46:41–50. https://doi.org/10.1515/mipo-2016-0006

Malaspina N, Hermann J, Scambelluri M, Compagnoni R (2006) Polyphase inclusions in garnet-orthopyroxenite (Dabie Shan, China) as monitors for metasomatism and fluid-related trace element transfer in subduction zone peridotite. Earth Planet Sci Lett 249:173–187. https://doi.org/10.1016/j.epsl.2006.07.017

Malaspina N, Hermann J, Scambelluri M (2009) Fluid/mineral interaction in UHP garnet peridotite. Lithos 107:38–52. https://doi.org/10.1016/j.lithos.2008.07.006

Malaspina N, Alvaro M, Campione M, Wilhelm H, Nestola F (2015) Dynamics of mineral crystallization from precipitated slab-derived fluid phase: first in situ synchrotron X-ray measurements. Contrib Mineral Petrol 169:1–12. https://doi.org/10.1007/s00410-015-1121-z

Mandler BE, Grove TL (2016) Controls on the stability and composition of amphibole in the Earth's mantle. Contrib Mineral Petrol 171:68. https://doi.org/10.1007/s00410-016-1281-5

Manning CE (2004) The chemistry of subduction-zone fluids. Earth Planet Sci Lett 223:1–16. https://doi.org/10.1016/j.epsl.2004.04.030

Mansker WL, Ewing RC, Keil K (1979) Barian-titanian biotites in nephelinites from Oahu, Hawaii. Am Mineral 64:156–159

Manuella FC, Carbone S, Ottolini L, Gibilisco S (2012) Micro-Raman spectroscopy and SIMS characterization of oxykinoshitalite in an olivine nephelinite from the Hyblean Plateau (Sicily, Italy). Eur J Mineral 24:527–533. https://doi.org/10.1127/0935-1221/2012/0024-2191

Massonne H-J (2003) A comparison of the evolution of diamondiferous quartz-rich rocks from the Saxonian Erzgebirge and the Kokchetav Massif: are so-called diamondiferous gneisses magmatic rocks? Earth Planet Sci Lett 216:347–364. https://doi.org/10.1016/S0012-821X(03)00512-0

Massonne HJ, Burchard M (2000) Exotic minerals in eclogites from the Central Erzgebirge—evidence for fluid-rock interaction at UH metamorphic pressures. In: "Berichte der Deutschen Mineralogischen Gesellschaft". Beih z Eur J Mineral 12:122

Massonne H-J, Opitz J, Theye T, Nasir S (2013) Evolution of a very deeply subducted metasediment from As Sifah, northeastern coast of Oman. Lithos 156–159:171–185. https://doi.org/10.1016/j.lithos.2012.11.009

Medaris LG Jr, Wang H, Jelínek E, Mihaljevič M, Jakeš P (2005) Characteristics and origins of diverse Variscan peridotites in the Gföhl Nappe, Bohemian Massif, Czech Republic. Lithos 82:1–23. https://doi.org/10.1016/j.lithos.2004.12.004

Medaris G, Ackerman L, Jelínek E, Michels Z, Erban V, Kotková J (2015) Depletion, cryptic metasomatism, and modal mesatomatism (refertilization) of Variscan lithospheric mantle: evidence from major elements, trace elements, and Sr–Nd–Os isotopes in a Saxothuringian garnet peridotite. Lithos 226:81–97. https://doi.org/10.1016/j.lithos.2014.10.007

Merlet C (1994) An accurate computer correction program for quantitative electron probe microanalysis. Microchim Acta 114–115:363–376. https://doi.org/10.1007/BF01244563

Mlčoch B, Konopásek J (2010) Pre-Late Carboniferous geology along the contact of the Saxothuringian and Teplá-Barrandian zones in the area covered by younger sediments and volcanics (western Bohemian Massif, Czech Republic). J Geosci 55:137–150. https://doi.org/10.3190/jgeosci.068

Munoz JL, Swenson A (1981) Chloride-hydroxyl exchange in biotite and estimation of relative HCl/HF activities in hydrothermal fluids. Econ Geol 76:2212–2221. https://doi.org/10.2113/gsecongeo.76.8.2212

Naemura K, Yokoyama K, Hirajima T, Svojtka M (2008) Age determination of thorianite in phlogopite-bearing spinel-garnet peridotite in the Gföhl Unit, Moldanubian zone of the Bohemian Massif. J Mineral Petrol Sci 103:285–290. https://doi.org/10.2465/jmps.080331

Naemura K, Hirajima T, Svojtka M (2009) The pressure-temperature path and the origin of phlogopite in spinel-garnet peridotites from the Blanský Les Massif of the Moldanubian Zone, Czech Republic. J Petrol 50:1795–1827. https://doi.org/10.1093/petrology/egp052

Palme H, O'Neill H (2014) Cosmochemical estimates of mantle composition. In: Carlson RW (ed) Treatise on geochemistry, 2nd edn, vol 3. Elsevier, Oxford, pp 1–39

Pan Y, Fleet ME (1991) Barian feldspar and barian-chromian muscovite from the Hemlo area, Ontario. Can Mineral 29:481–498

Pattiaratch DB, Saari E, Sahama TG (1967) Anandite, a new barium iron silicate from Wilagedera, North Western Province, Ceylon. Mineral Mag 36:1–4. https://doi.org/10.1180/minmag.1967.036.277.01

Pettke T, Halter WE, Webster JD, Aigner-Torres M, Heinrich ChA (2004) Accurate quantification of melt inclusion chemistry by LA-ICPMS: a comparison with EMP and SIMS and advantages and possible limitations of these methods. Lithos 78:333–361. https://doi.org/10.1016/j.lithos.2004.06.011

Philippot P, Chevallier P, Chopin Ch, Dubessy J (1995) Fluid composition and evolution in coesite-bearing rocks (Dora-Maira massif, Western Alps): implications for element recycling during subduction. Contrib Mineral Petrol 121:29–44. https://doi.org/10.1007/s004100050088

Rollinson H, Mameri L, Barry T (2018) Polymineralic inclusions in mantle chromitites from the Oman ophiolite indicate a highly magnesian parental melt. Lithos 310–311:381–391. https://doi.org/10.1016/j.lithos.2018.04.024

Scambelluri M, van Roermund H, Pettke T (2010) Mantle wedge peridotites: fossil reservoirs of deep subduction zone processes. Inferences from high and ultrahigh-pressure rocks from Bardane (Western Norway) and Ulten (Italian Alps). Lithos 120:186–201. https://doi.org/10.1016/j.lithos.2010.03.001

Schmädicke E, Evans BW (1997) Garnet-bearing ultramafic rocks from the Erzgebirge, and their relation to other settings in the Bohemian Massif. Contrib Mineral Petrol 127:57–74. https://doi.org/10.1007/s004100050265

Schmädicke E, Okrusch M, Schmidt W (1992) Eclogite-facies rocks in the Saxonian Erzgebirge, Germany: high pressure metamorphism under contrasting P–T conditions. Contrib Mineral Petrol 110:226–241. https://doi.org/10.1007/BF00310740

Seifert W, Kampf H (1994) Ba-enrichment in phlogopite of a nephelinite from Bohemia. Eur J Mineral 6:497–502

Shaw CS, Penczak RS (1996) Barium and titanium-rich biotite and phlogopite from the western and eastern gabbro, Coldwell alkaline complex, northwestern Ontario. Can Mineral 34:967–975

Solie DN, Su SC (1987) An occurrence of Ba-rich micas from the Alaska Range. Am Mineral 72:995–999

Solovova IP, Girnis AV, Ryabchikov ID, Kononkova NN (2009) Mechanisms of formation of barium-rich phlogopite and strontium-rich apatite during the final stages of alkaline magma evolution. Geochem Int 47:578–591. https://doi.org/10.1134/S0016702909060044

Sorensen SS, Grossman JN, Perfit MR (1997) Phengite-hosted LILE enrichment in eclogite and related rocks: implications for fluid-mediated mass transfer in subduction zones and arc magma genesis. J Petrol 38:3–34. https://doi.org/10.1093/petroj/38.1.3

Spandler C, Pirard C (2013) Element recycling from subducting slabs to arc crust: a review. Lithos 170–171:208–223. https://doi.org/10.1016/j.lithos.2013.02.016

Taylor SR, McLennan SM (1985) The continental crust: its composition and evolution. Blackwell, London

Tracy RJ (1991) Ba-rich micas from the Franklin marble, Lime Crest and Sterling Hill, New Jersey. Am Mineral 76:1683–1693

Tracy RJ, Beard JS (2003) Manganoan kinoshitalite in Mn-rich marble and skarn from Virginia. Am Mineral 88:740–747. https://doi.org/10.2138/am-2003-5-603

Tumiati S, Godard G, Martin S, Klötzli U, Monticelli D (2007) Fluid-controlled crustal metasomatism within a high-pressure subducted mélange (Mt. Hochwart, Eastern Italian Alps). Lithos 94:148–167. https://doi.org/10.1016/j.lithos.2006.06.009

Tumiati S, Fumagalli P, Tinaboschi C, Poli S (2013) An experimental study on COH-bearing peridotite up to 3.2 GPa, and implications for crust-mantle recycling. J Petrol 54:453–479. https://doi.org/10.1093/petrology/egs074

van Roermund HLM, Carswell DA, Drury MR, Heijboer TC (2002) Microdiamond in a megacrystic garnet websterite pod from Bardane on the island of Fjørtoft, western Norway: evidence for diamond formation in mantle rocks during deep continental subduction. Geology 30:959–962. https://doi.org/10.1130/0091-7613(2002)030%3C0959:MIAMGW%3E2.0.CO;2

Volfinger M, Robert JL, Vielzeuf D, Neiva AMR (1985) Structural control of the chlorine content of OH-bearing silicates (micas and amphiboles). Geochim Cosmochim Acta 49:37–48. https://doi.org/10.1016/0016-7037(85)90189-9

Vrijmoed JC, Van Roermund HLM, Davies GR (2006) Evidence for diamond-grade ultra-high pressure metamorphism and fluid interaction in the Svartberget Fe–Ti garnet peridotite-websterite body, Western Gneiss Region, Norway. Mineral Petrol 88:381–405. https://doi.org/10.1007/s00710-006-0160-6

Vrijmoed JC, Smith DC, van Roermund HLM (2008) Raman confirmation of microdiamond in the Svartberget Fe^Ti type garnet peridotite, Western Gneiss Region, Western Norway. Terra Nova 20:295–301. https://doi.org/10.1111/j.1365-3121.2008.00820.x

Yoshii M, Maeda K (1975) Relations between barium content and the physical and optical properties in the manganoan phlogophite-kinoshitalite series. Mineral J 8:58–65. https://doi.org/10.2465/minerj.8.58

Yoshii M, Maeda K, Kato T, Watanabe T, Yui S, Kato A, Nagashima K (1973) Kinoshitalite, a new mineral from the Noda-Tamagawa mine, Iwate Prefecture. Chigaku Kenkyu 24:181–190 **(in Japanese)**

Zaccarini F, Stumpel EF, Garuti G (2004) Zirconolite and Zr–Th–U minerals in chromitites of the Finero complex, Western Alps, Italy: evidence for carbonatite-type metasomatism in a subcontinental mantle plume. Can Mineral 42:1825–1845. https://doi.org/10.2113/gscanmin.42.6.1825

Zanetti A, Mazzucchelli M, Rivalenti G, Vannucci R (1999) The Finero phlogopite-peridotite massif: an example of subduction-related metasomatism. Contrib Mineral Petrol 134:107–122. https://doi.org/10.1007/s004100050472

Zhang M, Suddaby P, Thompson RN, Dungan MA (1993) Barian–titanian phlogopite from potassic lavas in northwest China: chemistry, substitutions and paragenesis. Am Mineral 78:1056–1065

Zheng YF, Hermann J (2014) Geochemistry of continental subduction-zone fluids. Earth Planets Sp 66:93. https://doi.org/10.1186/1880-5981-66-93

Zulauf G, Dörr W, Fiala J, Kotková J, Maluski H, Valverde-Vaquero P (2002) Evidence for high-temperature diffusional creep preserved by rapid cooling of lower crust (North Bohemian shear zone, Czech Republic). Terra Nova 14:343–354. https://doi.org/10.1046/j.1365-3121.2002.00424.x

Zurevinski SE, Mitchell RH (2011) Highly evolved hypabyssal kimberlite sills from Wemindji, Quebec, Canada: insights into the process of flow differentiation in kimberlite magmas. Contrib Mineral Petrol 161:765–776. https://doi.org/10.1007/s00410-010-0561-8